Comparison of thermocouples surface measurements and infrared thermography for transport infrastructure thermal monitoring

Thibaud Toullier, Jean Dumoulin, L Mevel

▶ **To cite this version:**

Thibaud Toullier, Jean Dumoulin, L Mevel. Comparison of thermocouples surface measurements and infrared thermography for transport infrastructure thermal monitoring. AITA 2017 - Advanced Infrared Technology and Applications, Sep 2017, Quebec City, Canada. hal-02139133

HAL Id: hal-02139133
https://hal.science/hal-02139133

Submitted on 24 May 2019

HAL is a multi-disciplinary open access archive for the deposit and dissemination of scientific research documents, whether they are published or not. The documents may come from teaching and research institutions in France or abroad, or from public or private research centers.

L'archive ouverte pluridisciplinaire **HAL**, est destinée au dépôt et à la diffusion de documents scientifiques de niveau recherche, publiés ou non, émanant des établissements d'enseignement et de recherche français ou étrangers, des laboratoires publics ou privés.

COMPARISON OF THERMOCOUPLES SURFACE MEASUREMENTS AND INFRARED THERMOGRAPHY FOR TRANSPORT INFRASTRUCTURE THERMAL MONITORING

T. Toullier[1,2], J. Dumoulin[1,2], L. Mevel[1,2]

[1] Ifsttar, COSYS-SII, Route de Bouaye, F-44340, Bouguenais, France
[2] Inria, Équipe I4S, Campus de Beaulieu, F-35042 Rennes, France

This study is intended to the evaluation and improvement of instrumentation solutions for long term monitoring of new generation of transport infrastructures. A test site has been instrumented with thermocouples and an infrared thermographic system coupled with the monitoring of environmental parameters. A spatial reconstruction method is proposed. Measured data acquired on site and post-processed are analyzed through time. Finally, obtained results are commented and perspectives are proposed.

Introduction

Studies around new deicing or controlled temperature structures are conducted under the 5th Generation Road (R5G) project of IFSTTAR. In order to control such structures, new thermal monitoring solutions *in-situ*, low cost and robust are needed. The aim of this study is to evaluate and improve thermal instrumentation solutions for long-term monitoring. First studies on uncooled infrared cameras has been made on open traffic structures [4], with promising results. If thermocouples or even optics fibers meet the expectation of thermal monitoring, the instrumentation can be complex, with a risk of breaking during the operation. On the contrary, infrared thermography seems more simple to deploy and offers a temperature measurement on multiple points at the same time.

However, in such application context, additional measurements are needed in order to convert the radiative fluxes (in digital levels) to temperature. In fact, the computation of the temperature will depend on spatial and meteorological parameters and also on the own characteristics of the observed object. Therefore, a multi-sensor system has been instrumented in order to improve this conversion process [3]. Thanks to the development of new technologies and more efficient computation power (GPGPU), acquisition means enable the synchronization and the coupling of data in order to make the best use of infrared measurements. Nevertheless, camera positioning will have an impact on the temperature computation. Indeed, the projection of the 3D scene causes a non-constant resolution on the image. In such context, we study an infrared spatial calibration method by using the geometry of the scene which is applied to outdoors measurements. Then, thermographic infrared temperature measurements are compared with thermocouples measurements located at the structure's surface. The comparison is analyzed and commented. Finally, we propose to quantify the difference between the two methods in dynamic state.

Test site and related instrumentation

An experiment has been conducted on an instrumented road concrete section. Our measurement system gathers the temperature from the surface thermocouples, a weather station and fluxes at small and large wavelength. In parallel, the whole section is monitored with a FLIR SC655 thermal infrared camera (640 X 480 LWIR FPA).

The flux received by the thermal camera depends on its surrounding environmental conditions and also the thermo-optics properties of the measurement scene [4, 6]. Furthermore, the camera is placed on a mast, leading to a non-constant spatial sampling of the surface of the monitored scene. In such configuration, the radiation flux attenuated by the atmosphere depends on the position of the measurement point in the scene (Fig. 1).

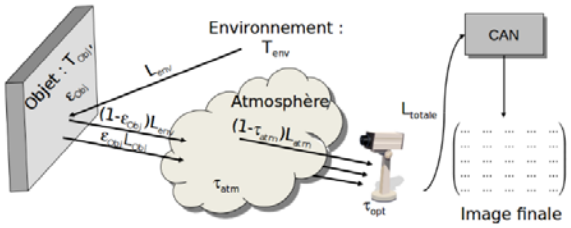

Figure 1. Illustration of the fluxes received by the camera

First, we can express for each point of the infrared image the total radiance L_{tot} by using the simplified radiometric equation to retrieve the flux received by the camera (Eq. 1)

$$\begin{aligned} L_{tot}^{i,j} &= \epsilon_{obj}\tau_{atm}\tau_{opt}L_{obj}^{i,j} \\ &+ \left(1-\epsilon_{obj}\right)L_{env}\tau_{atm}\tau_{opt} \\ &+ (1-\tau_{atm})L_{atm}\tau_{opt} \\ &+ L_{opt}\left(1-\tau_{opt}\right) \end{aligned} \quad (1)$$

From this equation, we can retrieve the self-radiative contribution of our object. As mentioned before, the weather station is used to compute the environmental quantities from equation 1. The reflected, optics and atmospherics radiance values are computed by injecting some knowledge about the monitored objects, components of the infrared system and atmospherics conditions. For example, the atmospheric transmission τ_{atm} is function of the point within the image, external temperature and relative humidity.

Prior to the experiment, a thermal calibration is performed in order to retrieve the temperature as a function of the digital level associated to the radiance for each pixel of the image, following the equation 2.

$$T_{obj} = \frac{B}{\log\left(\frac{R}{L_{obj}}\right)+F} \quad (2)$$

Where R, B and F are calibration constants. Equation 1 shows the strong interaction between our measurement system and the environment. The uncertainty due to the estimation of transmittance, emissivity and atmospheric radiances will influence the final result in a non-negligible way [2]. As shown by [8] in their simulation, solar flux, sky temperature or even rainfall are all parameters that can be a source of error when converting infrared measurements into temperature. Camera's position will also influence the calculation of the temperature which depends on the angle and the distance between the camera and the observed object. In the following, we propose a method for calibrating the image in order to extract at best thermal data to make a comparison with the thermocouples measurements.

Camera resectioning

In order to solve the simplified radiometric equation, the knowledge of spatial parameters is needed. The Direct Linear Transformation (DLT) [5] algorithm has been used on the measurements on site. The objective is to get the correspondences between the original coordinates and the image coordinates (Fig. 2).

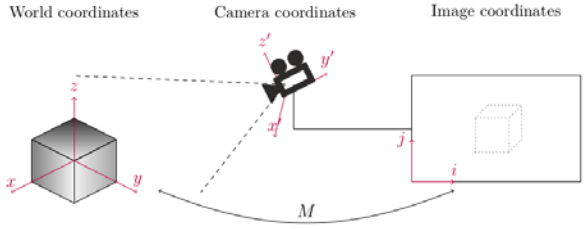

Figure 2. Illustration of a scene setup

We want to find the matrix M so that for every couple $(x, X) \in \mathbb{R}^2 \times \mathbb{R}^3$:

$$x = MX \quad (3)$$

M can be expressed in homogeneous coordinates as:

$$M = \begin{pmatrix} f & s_k & c_x \\ 0 & af & c_y \\ 0 & 0 & 1 \end{pmatrix} \begin{pmatrix} 1 & 0 & 0 & 0 \\ 0 & 1 & 0 & 0 \\ 0 & 0 & 1 & 0 \end{pmatrix} \begin{pmatrix} R_{3\times3} & 0_{3\times1} \\ 0_{1\times3} & 1 \end{pmatrix} \begin{pmatrix} I_3 & T_{3\times1} \\ 0_{1\times3} & 1 \end{pmatrix} \quad (4)$$

This system has 11 degrees of freedom, so it is necessary to know at least the coordinates associated to 6 points in order to solve it. Those 6 points are normalized so that:

- The barycenter of the two sets of points are at the origin

- The points are in average around the unit ball in their space in euclidian norm.

Therefore, two normalization matrices (U and V) are defined:

$$\hat{X}_i = UX_i, \hat{x}_i = Vx_i \quad (5)$$

The Levenberg-Marquardt algorithm is used to minimize the geometric error (Eq. 6) [1]. In order to approach the solution, the algorithm is initialized with the result of a singular value decomposition.

$$\min \sum_{1 \le i \le N} d(\hat{x}_i, M\hat{X}_i) \quad (6)$$

The jacobian matrix for the Levenberg-Marquardt algorithm is analytically calculated (Eq. 7)

$$J_M = \frac{\partial(\hat{u}-u, \hat{v}-v, 1-s)}{\partial(f, a, c_x, c_y, s_k, t_x, t_y, t_z, w_x, w_y, w_z)} \quad (7)$$

Where $T = (t_x, t_y, t_z)$ and $W = (w_x, w_y, w_z)$ are respectively the translation and the rotation matrices. W is obtained with the Rodrigues rotation formula.

Once calibrated, a distance map and an angle map are computed and can be injected to our computation model (Fig. 3). This distance map is not yet integrated into the computation of the atmospheric transmission but we can note that regarding our setup (12m at maximum) the distance has a low impact on the final result, compared to the environmental conditions (relative humidity evolution through time for example). Those two maps enable us to perform geometrical transformations on the images and compare them with the thermocouples measurements.

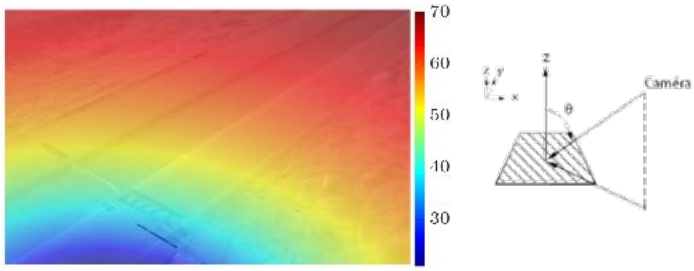

Figure 3. Angle map (degrees) and the angle definition

The result of image rectification is given in figure 4.

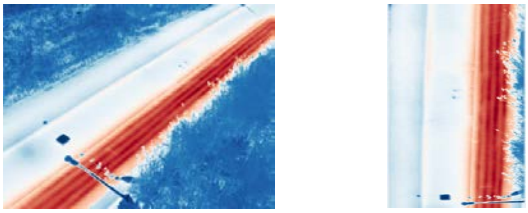

Figure 4. Original image (left) and rectified image (right)

Results analysis

The Figure 5 shows a comparison of two measured signals, one with surface thermocouple and the other one by data extraction on the rectified image with the model presented in the previous section. After calibration, the thermocouples position on the image enables us to extract the temperature values on the image sequence to recreate the thermal signal for a given period. A statistical comparison of the two times signals shows that the signals can be relatively close (expected value of $0.70°C$ and standard deviation of $0.69°C$), the difference is not null and can be important on specific periods of time (for example due to the presence of hydrometeors).

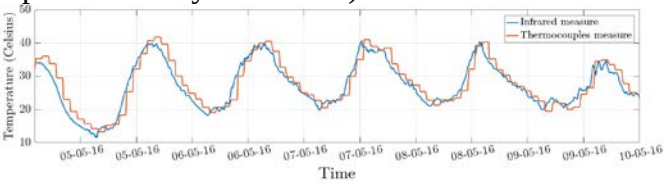

Figure 5. Infrared measurements compared to thermocouples measurements

To analyze more deeply the differences and evaluate the robustness of the infrared measure, the Dynamic Time Warping (DTW) algorithm has been used [7]. This algorithm optimizes the alignment of two temporal observations by minimizing the distance between every points. The computed distance gives information on the similitude of the two signals. By computing the distance DTW locally between the thermocouple and infrared measure, we can see the impact of the outdoor conditions on the infrared measurement.

To do so, let $X = (x_i)$ and $Y = (y_i), 1 \le i \le N, 1 \le j \le M$ be our two observations. We initialize the matrix dtw such as:

$$dtw(i,j) = \begin{cases} \infty & \text{if i=0 or } j = 0 \\ 0 & \text{if i=j=0} \end{cases} \quad (8)$$

The distance DTW is then computed in dynamic programming by defining a cost function $c(x_i, y_j)$

$$dtw(i,j) = c(x_i, y_i) + \min \begin{cases} dtw(i-1, j-1) \\ dtw(i-1, j) \\ dtw(i, j-1) \end{cases} \quad (9)$$

For $1 < i < N, 1 < j < M$ and $|i - j| < w$ where w represents the maximum temporal tolerance between the two signals. In our case, the DTW distance has been computed by narrowing a region of interest with a sliding window. We have defined a six hours observation window and admitted a maximal offset between the signals (w) of ± 2 hours. The cost function chosen was the euclidian distance. Finally, the final value was divided by the size of our observation window in order to get an average value. This method helps us to quantify the difference between the different methods for a given period, and close experimental conditions.

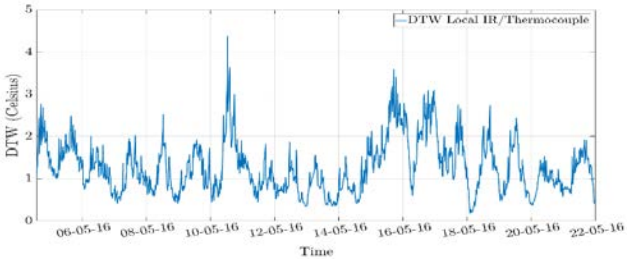

Figure 6. Comparison between the infrared thermogram and the related thermocouple signal with the DTW algorithm

Therefore, we can observe that the similitude between the two signals will be more or less important depending on the considered period (Fig. 6). The peaks that we can observe on this figure correspond to rainfall episodes for which the impact has to be considered in the correction process for outdoors infrared thermographic measurements.

Conclusion

A conversion in temperature from digital levels for infrared thermography coupled to a rectification algorithm has been presented in this study. The computed temperatures has been compared to measurements made with thermocouples on the concretes' surface. The rectification algorithm enabled us to extract thermal profiles of interest and to correct some projection errors. If differences exist between the two methods, the results are encouraging. In fact, infrared cameras can measure the temperature in multiple points on the scene, which is difficult to reproduce with thermocouples. This study highlighted issues with long-term thermal monitoring with spatial and temporal resolutions that are different than airborne or satellite systems (due to scale difference). Some improvements are possible for the computation model we use. Indeed, our experiment enabled us to collect and synchronize numerous data, thermal, meteorological and solar. We will pursue the study of those data in order to refine our model and take into account different meteorological conditions.

References

1. Edwin K. P. Chong and Stanislaw H. Zak. An Introduction to Optimization. Wiley-Blackwell, Hoboken, New Jersey, 4th edition edition, February 2013.
2. K. Chrzanowski. Influence of measurement conditions and system parameters on accuracy of remote temperature measurement with dualspectral IR systems. Infrared Physics & Technology, (37) :295–306, 1996.
3. Jean Dumoulin and Vincent Boucher. Infrared thermography system for transport infrastructures survey with inline local atmospheric parameter measurements and offline model for radiation attenuation evaluations. Journal of Applied Remote Sensing, 8(1) :084978–084978, 2014.
4. Jean Dumoulin, Antoine Crinière, and Rodolphe Averty. The detection and thermal characterization of the inner structure of the 'Musmeci' bridge deck by infrared thermography monitoring. Journal of Geophysics and Engineering, 10(6) :064003, December 2013.
5. Richard Hartley and Andrew Zisserman. Multiple View Geometry in Computer Vision. Cambridge University Press, Cambridge, UK ; New York, 2 edition edition, April 2004.
6. J.R. Howell, R. Siegel, and M.P. Pinar. Thermal Radiation Heat Transfer. CRC Press, 5th edition, 2010.
7. Diego F. Silva and Gustavo EAPA Batista. Speeding up all-pairwise dynamic time warping matrix calculation. In Proceedings of the 2016 SIAM International Conference on Data Mining, pages 837–845. SIAM, 2016.
8. Sven Van De Vijver, Marijke Steeman, Nathan Van Den Bossche, Kim Carbonez, and Arnold Janssens. The influence of environmental parameters on the thermographic analysis of the building envelope. In 12th International Conference on Quantitative InfraRed Thermography (QIRT 2014), 2014.